Applied Surface Science 258 (2012) 7094–7098

Contents lists available at SciVerse ScienceDirect

Applied Surface Science

journal homepage: www.elsevier.com/locate/apsusc

Temperature dependent field emission performances of carbon nanotube arrays: Speculation on oxygen desorption and defect annealing

Jian-hua Deng, Yu-mei Yang, Rui-ting Zheng, Guo-an Cheng*

Key Laboratory of Beam Technology and Material Modification of the Ministry of Education, College of Nuclear Science and Technology, Beijing Normal University, Beijing 100875, People's Republic of China

ARTICLE INFO

Article history:
Received 19 November 2011
Received in revised form 9 March 2012
Accepted 31 March 2012
Available online 6 April 2012

Keywords:
Multi-walled carbon nanotubes
Temperature
Field emission
Oxygen desorption
Annealing

ABSTRACT

We report here a systematic study of the field emission (FE) properties of highly ordered carbon nanotube (CNT) arrays at different temperatures. The FE characteristics of the CNT arrays are significantly improved with temperature increasing from 298 K to 473 K, as evidenced by the decreases of turn-on electric field at 10 μA/cm^2 from 1.064 to 0.774 V/μm and threshold field at 10 mA/cm^2 from 1.628 to 1.418 V/μm, respectively. Moreover, the stability behavior of the CNT arrays is ameliorated at or after suffering to temperatures. Raman, EDS, XPS, and photoelectron spectrometer were employed to characterize the CNT arrays before and after the FE-Temperature measurements for comparison. Our results demonstrate that the oxygen desorption induced work function decrease (from 4.89 to 4.68 eV) of the CNT arrays after longtime exposure to temperature is responsible for the improved FE behavior, while the annealing of defects on CNTs is the main reason for the improved FE stability, which provides an effective approach to stabilizing emitters by temperature processing.

1. Introduction

Since the first demonstration of carbon nanotubes (CNTs) as field emitters in 1995 [1], the interest in these structures has been recurrent, and substantial studies have been focused on exploring applications due to their outstanding electronic and mechanical characteristics [2–7]. Owing to the large aspect ratio (h/r, where h is the length and r is the radius of tubes, respectively) of CNT, it is possible to achieve extremely large local applied fields ($E_{loc} = \beta V/d$, where β is the enhancement factor of CNT, calculated by $\beta = h/r$, V and d are the applied voltage and the distance between the anode and the emitters, respectively) at its emission sites, ensuring a significant tunneling of electrons through CNT barriers. In this regard, CNTs show excellent field emission (FE) properties with low turn-on electric field (E_{on}, applied field at 10 μA/cm^2) and threshold field (E_{th}, applied field at 10 mA/cm^2), far better than that of some other low dimensional field electron emitting materials like nanofibers [8], nanorods [9], nanotips [10], and single-layer graphene [11], making them good candidates in applications as high-performance FE electron sources for flat panel displays [12,13], lamps [14], X-ray tubes [15–17], and ultra-high luminance light-source devices [18].

However, most of the FE measurements of CNTs so far are performed at room temperature (RT), and only a few studies are carried out at higher temperatures. Tan et al. showed that the FE properties of CNTs were temperature dependent when the temperature was above 373 K owing to their temperature dependent work function changes [19]. Das et al. showed similar temperature dependence of FE from CNTs and discussed it from the morphology change (aspect ratio) of emitters [20]. Chen et al. observed that the emission current increased considerably due to a direct heating process on the emitters [21]. FE at higher temperatures is important in practical applications, such as in FE electron microscopes for *in situ* engineering products in a high temperature ambient. Besides, the exact mechanisms of this temperature dependent FE need to be further understood.

Here we report the FE behavior of highly ordered multi-walled CNTs at temperatures ranging from RT to 200 °C, systematically discuss the FE dependence of the CNT arrays on temperature from the change of work function, oxygen desorption, and defect annealing.

2. Experimental details

2.1. Preparation and structural characterization of the CNT arrays

Synthesizing CNT arrays by using thermal chemical vapor deposition has been discussed previously in detail [22]. First, 5-nm-thick iron film was deposited on Si wafers as the catalyst using magnetron sputtering. Then the catalyst was annealed at 580 °C for 1 h under 400 sccm H_2 in a tubular furnace. Before the growth, the catalyst was etched in 150 sccm NH_3 for 10 min at 750 °C. The growth

* Corresponding author. Tel.: +86 010 62205403; fax: +86 010 62205403.
E-mail address: gacheng@bnu.edu.cn (G.-a. Cheng).

0169-4332/$ – see front matter © 2012 Elsevier B.V. All rights reserved.
http://dx.doi.org/10.1016/j.apsusc.2012.03.184

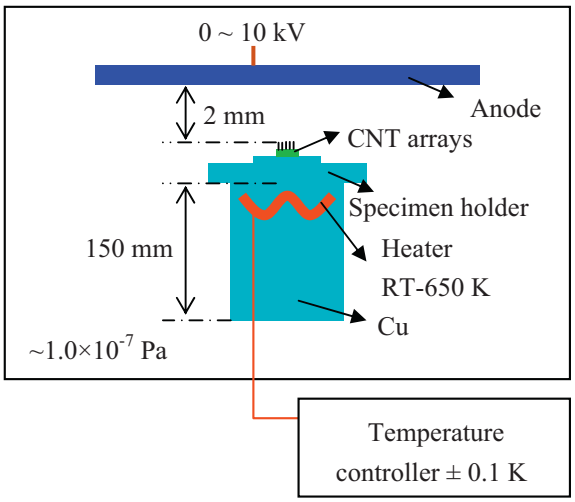

Fig. 1. Schematic of the diode setup used for FE measurements at different temperatures.

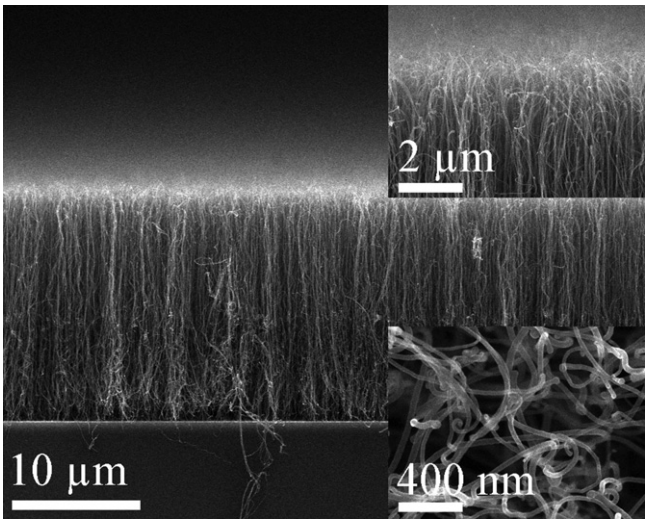

Fig. 2. SEM images of the as-grown CNT arrays.

was then carried out at 750 °C for 30 min under a gas mixture of 600 sccm H_2 and 87 sccm C_2H_2. After then, the sample was rapidly cooled to RT in H_2 ambient (600 sccm).

The surface morphology of the CNT arrays was examined by scanning electron microscope (SEM, Hitachi S-4800, 10 kV). Raman (633 nm, LobRAM Aramis), energy dispersive X-ray spectroscopy (EDS, Hitachi S-4800), X-ray energy photoelectron spectrometer (XPS, PHI Quantera SXM) were used to characterize the CNT arrays before and after the FE measurements for comparison. The work function of the CNT arrays was determined by photoelectron spectrometer (AC-2 RIKEM KEIKI) in ambient pressure at room temperature, and a detailed description of the method used for work function measurements is shown in Supplementary information (Method for work function measurements and Fig. S1).

2.2. Field emission characterization of the CNT arrays at different temperatures

The FE measurements were carried out using a diode setup in vacuum (~1.0×10^{-7} Pa), as schematically shown in Fig. 1. The CNT arrays were used as the cathode and a stainless steel plate (~100 mm in diameter) was used as the anode, and the distance between the cathode and the anode (A–C distance) was 2 mm. A heater was placed in the copper cylinder (~150 mm in height) and controlled by a temperature controller (±1 K). During FE-Temperature (FE-T) measurements, the height of the copper cylinder changes with temperatures, bringing changes to the A-C distance, either. To keep the A–C distance unchanged during all our FE tests, we developed a device to adjust this temperature induced experimental error, and the detailed method is shown in Supplementary information (Method for FE-Temperature measurements and Fig. S2). The emission current and applied voltage (*I*–*V*) was recorded automatically by a computer program, and the increasing rate of the applied voltage was 500 V/min.

3. Results and discussion

3.1. SEM characterization of the CNT arrays

The representative morphologies of the CNT arrays were investigated by SEM, as shown in Fig. 2. It can be observed that the CNTs are orderly aligned on the Si substrates with ~20 μm in length and 30–50 nm in diameter, and densely packed but nonetheless the CNT tips are well separated with each other (Fig. 2a, insets). Unlike the other sections of the CNTs which are nearly straight, the CNT tips are curled owing to a CNT density decrease induced reduction of the van der Waals force. These curled and low-density natures of the CNT tips can weaken the influence of field-screening so to improve the FE behavior of emitters [23], but then, these less field screened emitters are supposed to suffer much more emission current and therefore more likely to be burned off by Joule heat during FE, resulting in FE degradation [24–27].

3.2. FE behavior of the CNT arrays at different temperatures

We respectively tested the FE behavior of the CNT arrays at 298 K, 373 K, 473 K and 298 K after the above FE-T tests (a-298 K) at a constant 2 mm gap between the anode and a sample, as shown in Fig. 3. The data is plotted as emission current density (*J*) versus applied field (*E*), namely, *J*–*E* plots. a-298 K aside, the FE properties of the CNT arrays are improved gradually as temperature increasing, which can be seen from the left-shift of *J*–*E* plots. The great decreases of E_{on} from 1.064 to 0.774 V/μm and E_{th} from 1.628 to 1.418 V/μm after increasing temperature from RT (~298 K) to 473 K can fully express this FE improvement of the CNT arrays (Table 1).

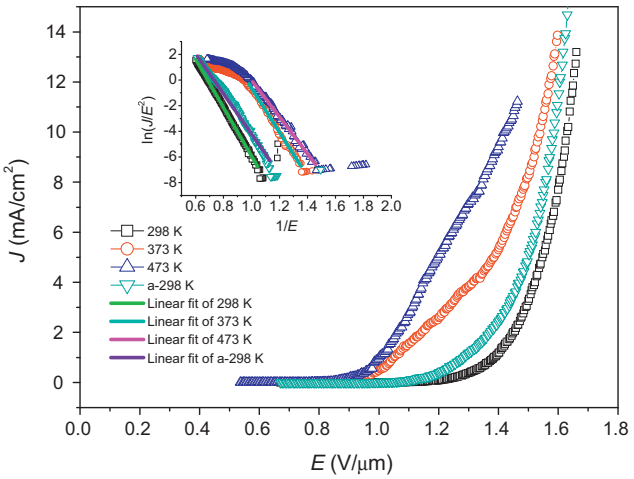

Fig. 3. FE behavior of the CNT arrays at 298 K, 373 K, 473 K and a-298 K (298 K but after the FE-Temperature tests), respectively, given in terms of emission current density (*J*) versus applied field (*E*), the inset is the corresponding F–N plots.

Table 1
Field emission results of the CNT arrays at different temperatures.

Temperature (K)	Turn-on electric field (V/μm)	Threshold field (V/μm)	Work function (eV)	Field enhancement factor
298	1.064	1.628	4.89	3909
373	0.836	1.539	–	4013–4286
473	0.774	1.418	–	4824–5152
a-298	0.985	1.587	4.68	4415

To understand the physical mechanism underlying, we re-plot the J–E data in terms of $\ln(J/E^2)$ versus $1/E$, so called Fowler–Nordheim (F–N) plots [28], as shown in the inset of Fig. 3. The linear variation of these F–N plots in the low field region suggests that electron emission from the CNTs follows the F–N theory when the applied field is low [11,28]. We further measured the work function (Φ) of the CNT arrays using a photoelectron spectrometer to determine their field enhancement factors (β) [28]. Since it is difficult to perform an *in situ* measurement on the samples during FE, the Φ was measured before and immediately after the FE-T tests at RT for comparison, which is 4.89 eV for the as-grown (298 K) and 4.68 eV for the temperature suffered CNT arrays (a-298 K), indicating a temperature processing induced work function decrease. Since 373 K and 473 K are intermediate states between the initial (298 K) and the final (a-298 K) states, it is reasonable to assume that the work functions of the CNT arrays at 373 K and 473 K are between 4.89 eV and 4.68 eV, so the β from the F–N plots can be calculated, as summarized in Table 1. CNT arrays at 473 K have the highest β value (4824–5152) compared to 298 K (~3909), 373 K (4013–4286) and a-298 K (~4415). Therefore, the excellent FE behavior of the CNT arrays at 473 K is likely attributed to the higher aspect ratio (β) and the decreased work function than that at other temperatures.

Fig. 4 shows FE stability behavior of the CNT arrays around ~10 mA/cm^2 at different temperatures, evaluated by a parameter J_{drop}, given by $(J_{starting} - J_{last})/J_m$, where $J_{starting}$, J_{last} and J_m are the first, the last and the mean emission current density during the stability measurements, respectively, and "+" for current increase and "−" for current decrease. Compared to the CNT arrays at RT (J_{drop} = −12.34%), the J_{drop} of the CNT arrays decreases at other temperatures (less than +5.93%). The smallest J_{drop} is obtained for CNT arrays after those FE-T tests (+0.39%), suggesting an effective approach to ameliorating the stability of emitters by longtime exposure to temperatures. Moreover, the emission current increases, roughly in the first 2 h, when the temperature is non-RT

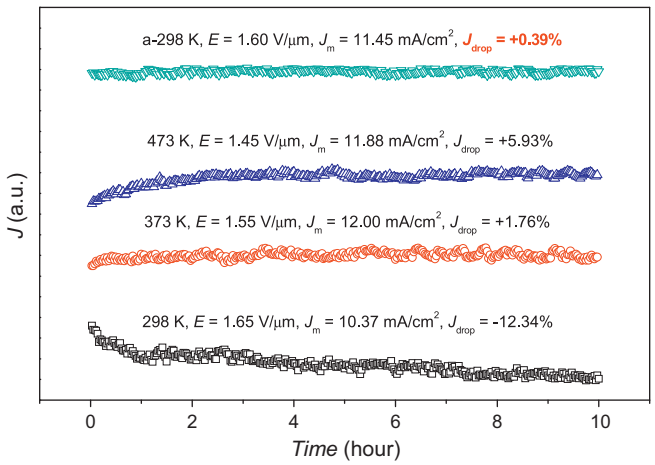

Fig. 4. FE stability of the CNT arrays around ~10 mA/cm^2 at 298 K, 373 K, 473 K, and a-298 K, respectively. E, J_m and J_{drop} are applied fields during stability tests, mean emission current density and current degradation during the testing time, respectively. "+" for current increase and "−" for current decrease.

(Fig. 4), which can be ascribed to a competition between Joule heating induced current degradation [24–27] and temperature processing induced FE improvement. In thinking that thermoion current is negligible under 1000 K in comparison with FE current [19,29], not to mention temperatures in our study (less than 500 K), we ascribe the improved FE of the CNT arrays to oxygen desorption and defect annealing, since oxygen desorption is supposed to decrease the work function of emitters while annealing of defects is beneficial for ameliorating the FE stability of emitters by weakening Joule heating induced emitter burn-off [24–27].

3.3. Oxygen desorption and defect annealing of CNTs under temperatures

CNT arrays at the initial (298 K) and the final (a-298 K) states were measured for comparison using EDS, XPS and Raman, as shown in Fig. 5. Fig. 5a shows XPS spectra of the CNT arrays with binding energy ranges from 0 to 1100 eV. Typical O1s peak centered at ~532 eV is clearly observed in the XPS spectrum of the as-grown CNT arrays before FE-T tests, which is corresponding with oxygen contaminants like C=O [30] and C—O [31]. The O1s peak becomes quite weak in the XPS spectrum of the a-298 K sample, indicating oxygen desorption during the FE-T tests. Further oxygen desorption evidence was obtained in the EDS observation, as shown in the inset of Fig. 5a. The atomic percentage (at%) of oxygen of the CNT arrays decreases from 6 to 8% to less than 2% after the long-time exposure to temperature. Fig. 5b shows the fitted results of the C1s peak of the CNT arrays after FE-T tests. The C1s peak centers at ~284.1 eV in the 298 K curve while at ~283.6 eV in the a-298 K curve, this 0.5 eV left shift (inset of Fig. 5b, marked by a red arrow) of the C1s peak can also confirm the oxygen desorption. In a C—O system, C—O bonds make carbon positively charged while oxygen negatively charged, resulting in an increase of binding energy in carbon and a decrease of binding energy in oxygen, it is therefore no wonder that the binging energy of C1s peak decreases after the oxygen desorption. Combining with the FE properties of the CNT arrays shown in Fig. 3 and Table 1, the decreased binding energy of carbon induced by oxygen desorption is supposed to ascend the Fermi Lever, yielding the decrease of work function (from 4.89 to 4.68 eV), which is beneficial for decreasing the electron tunneling barriers during FE and improving the FE behavior of emitters.

Information on structural evolution can also be obtained from the fitted results of the XPS C1s peaks of the CNT arrays (Fig. 5b). Three peaks centered at ~283.5 eV, ~284.8 eV and ~288 eV are corresponding with graphite carbon [32], diamond-like carbon [33] and organic contaminated carbon [34], respectively. We use the percentage of SP^2-hybridized carbon (SP^2%) to evaluate the crystallinity of the CNT arrays and find that SP^2% increases from 60.52% to 70.16% after the longtime FE-T measurements, indicating that part of intrinsic defects of the CNTs have been annealed even the temperature is not high (less than 500 K). Further insights of the structural evolution were obtained from the Raman spectra of the CNT arrays, as shown in Fig. 5c. Two typical carbon-related Raman peaks, defective carbon related D band around 1331 cm^{-1} and graphite carbon related G band around 1580 cm^{-1}, are obtained in both Raman spectra and further confirm that our CNTs are defective [35]. The slight decrease of the intensity ratio between D peak and G

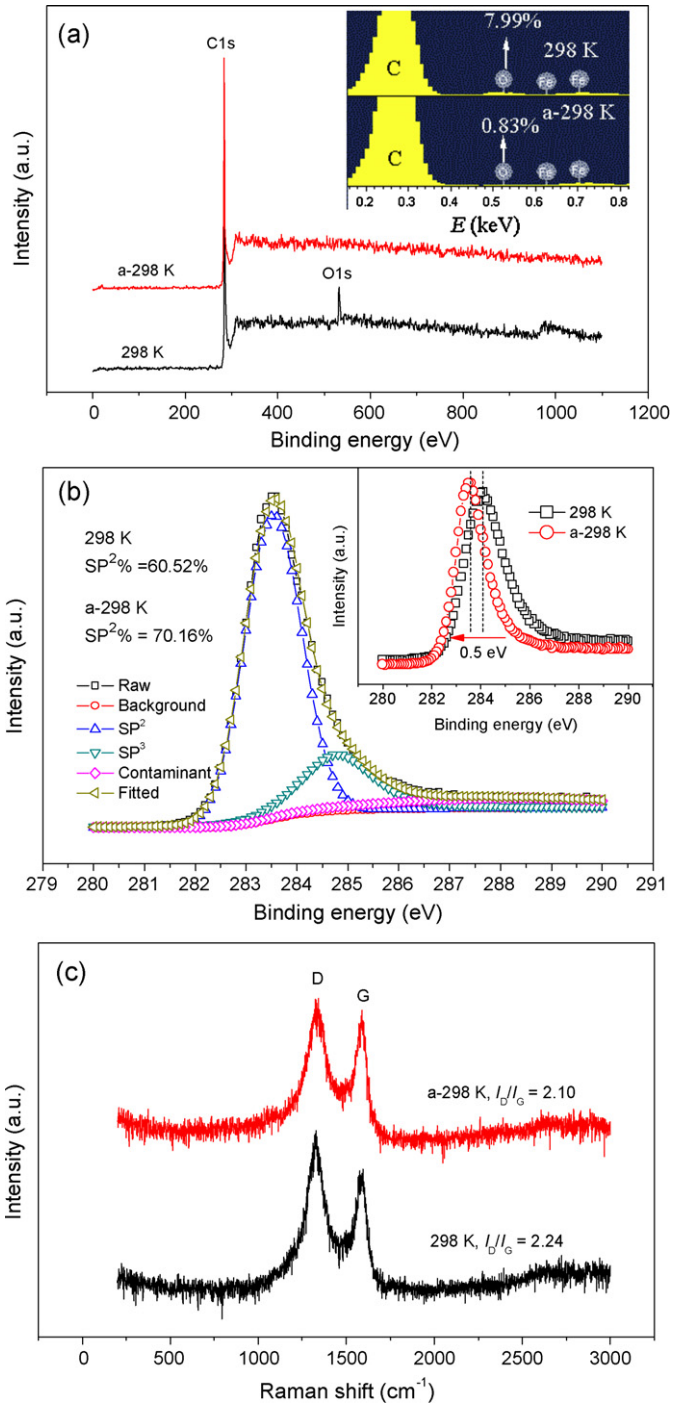

Fig. 5. (a) XPS spectra, EDS spectra (inset), (b) a-298 K C1s peak decomposition, raw C1s peaks (inset), and (c) Raman spectra of the as-grown CNT arrays before (298 K) and after (a-298 K) the FE-T tests. The percentage shown in the inset of (a) is at%. I_D and I_G in (c) respectively correspond with the intensity of Raman D peak and G peak.

peak (I_D/I_G) after the FE-T tests is another evidence for the annealing of defects. Defects, especially vacancy-related defects, increase emission current by providing more effective electron transmission traces, so the annealing of defects is detrimental to FE (which is only related to the *J–E* behavior) [36,37]. However, compared to oxygen desorption induced FE improvement, this defect annealing induced FE degradation is negligible, the *J–E* plots still shift to the low applied field region (left-shift shown in Fig. 3). On the other hand, annealing of defects is beneficial for improving the stability behavior of emitters in a way of reinforcing the defective locations which are more likely to be burned off by Joule heat during FE [24–27]. The competition between oxygen desorption induced FE improvement and defect annealing induced FE degradation determines the stability behavior of the CNT arrays at 373 K and 473 K (Fig. 4) until they reach a balance in a few hours, after then, the field emission advances stably.

4. Conclusions

We have demonstrated a systematic study of the FE properties of as-grown CNT arrays at different temperatures. We found that the FE behavior of the CNT arrays was improved after increasing temperature from 298 K to 473 K, clearly evidenced by the great decreases of E_{on} from 1.064 to 0.774 V/μm and E_{th} from 1.628 to 1.418 V/μm, and the stability was improved, either. Basing on analyses from EDS, XPS and Raman, we ascribed the improved FE of the CNT arrays to the oxygen desorption induced decrease of work function from (4.89 to 4.68 eV), while the improved stability is due to defect annealing which can stabilize the emitters. Our results have provided an effective approach to ameliorating FE behavior of emitters by high-temperature annealing.

Acknowledgments

This work was supported by the National Basic Research Program of China (no. 2010CB832905), and partially by the Key Scientific and Technological Project of the Ministry of Education of China (no. 108124).

Appendix A. Supplementary data

Supplementary data associated with this article can be found, in the online version, at http://dx.doi.org/10.1016/j.apsusc.2012.03.184.

References

[1] W.A. de Heer, A. Châtelain, D. Ugarte, A carbon nanotube field-emission electron source, Science 270 (1995) 1179–1180.
[2] S.S. Fan, M.G. Chapline, N.R. Franklin, T.W. Tombler, A.M. Cassell, H.J. Dai, Self-oriented regular arrays of carbon nanotubes and their field emission properties, Science 283 (1999) 512–514.
[3] L.B. Zhu, Y.Y. Sun, D.W. Hess, C.P. Wong, Well-aligned open-ended carbon nanotube architectures: an approach for device assembly, Nano Letters 6 (2006) 243–247.
[4] J.M. Bonard, N. Weiss, H. Kind, T. Stöckli, L. Forró, K. Kern, A. Châtelain, Tuning the field emission properties of patterned carbon nanotube films, Advanced Materials 13 (2001) 184–188.
[5] P. Hojati-Talemi, G.P. Simon, Enhancement of field emission of carbon nanotubes using a simple microwave plasma method, Carbon 49 (2011) 484–486.
[6] A.G. Rinzler, J.H. Hafner, P. Nikolaev, L. Lou, S.G. Kim, D. Tomanek, P. Nordlander, D.T. Colbert, R.E. Smalley, Unraveling nanotubes: field emission from an atomic wire, Science 269 (1995) 1550–1553.
[7] R.H. Baughman, A.A. Zakhidov, W.A. de Heer, Carbon nanotubes—the route toward applications, Science 297 (2002) 787–792.
[8] C.H. Weng, K.C. Leou, H.W. Wei, Z.Y. Juang, M.T. Wei, C.H. Tung, C.H. Tsai, Structural transformation and field emission enhancement of carbon nanofibers by energetic argon plasma post-treatment, Applied Physics Letters 85 (2004) 4732–4734.
[9] R.C. Che, M. Takeguchi, M. Shimojo, K. Furuya, Field electron emission from single carbon nanorod fabricated by electron beam induced deposition, Journal of Physics: Conference Series 61 (2007) 200–204.
[10] C.L. Tsai, C.F. Chen, L.K. Wu, Bias effect on the growth of carbon nanotips using microwave plasma chemical vapor deposition, Applied Physics Letters 81 (2002) 721–723.
[11] Z.M. Xiao, J.C. She, S.Z. Deng, Z.K. Tang, Z.B. Li, J.M. Lu, N.S. Xu, Field electron emission characteristics and physical mechanism of individual single-layer graphene, ACS Nano 4 (2010) 6332–6336.
[12] Q.H. Wang, M. Yan, R.P.H. Chang, Flat panel display prototype using gated carbon nanotube field emitters, Applied Physics Letters 78 (2001) 1294–1296.
[13] N.S. Lee, D.S. Chung, I.T. Han, J.H. Kang, Y.S. Choi, H.Y. Kim, S.H. Park, Y.W. Jin, W.K. Yi, M.J. Yun, J.E. Jung, C.J. Lee, J.H. You, S.H. Jo, C.G. Lee, J.M. Kim, Application

of carbon nanotubes to field emission displays, Diamond and Related Materials 10 (2001) 265–270.
[14] Y. Saito, S. Uemura, Field emission from carbon nanotubes and its application to electron sources, Carbon 38 (2000) 169–182.
[15] G.Z. Yue, Q. Qiu, B. Gao, Y. Cheng, J. Zhang, H. Shimoda, S. Chang, J.P. Lu, O. Zhou, Generation of continuous and pulsed diagnostic imaging x-ray radiation using a carbon-nanotube-based field-emission cathode, Applied Physics Letters 81 (2002) 355–357.
[16] H. Sugie, M. Tanemura, V. Filip, K. Iwata, K. Takahashi, F. Okuyanma, Carbon nanotubes as electron source in an x-ray tube, Applied Physics Letters 78 (2001) 2578–2580.
[17] A. Haga, S. Senda, Y. Sakai, Y. Mizuta, S. Kita, F. Okuyama, A miniature X-ray tube, Applied Physics Letters 84 (2004) 2208–2210.
[18] Y. Saito, K. Hata, A. Takakura, J. Yotani, S. Uemura, Field emission of carbon nanotubes and its application as electron sources of ultra-high luminance light-source devices, Physica B 323 (2002) 30–37.
[19] C.M. Tan, J.J. Jia, W.B. Yu, Temperature dependence of the field emission of multiwalled carbon nanotubes, Applied Physics Letters 86 (2005) 263104.
[20] S. Das, S.F. Ahmed, M.K. Mitra, K.K. Chattopadhyay, Morphology and temperature-dependent electron field emission from vertically aligned carbon nanfibers, Applied Physics A 91 (2008) 429–433.
[21] Y.C. Chen, H.F. Cheng, Y.S. Hsieh, Y.M. Tsau, Electron field emission properties of carbon nanotubes during thermal heating and laser irradiation, Journal of Applied Physics 94 (2003) 7739–7742.
[22] J.H. Deng, Z.X. Ping, R.T. Zheng, G.A. Cheng, Electron transferring from titanium ion irradiated carbon nanotube arrays into vacuum under low applied fields, Nuclear Instruments and Methods in Physics Research Section B 269 (2011) 1082–1087.
[23] J.S. Suh, K.S. Jeong, J.S. Lee, I. Han, Study of the field-screening effect of highly ordered carbon nanotube arrays, Applied Physics Letters 80 (2002) 2392–2394.
[24] Z.S. Wu, S.F. Pei, W.C. Ren, D.M. Tang, L.B. Gao, B.L. Liu, F. Li, C. Liu, H.M. Cheng, Field emission of single-layer graphene films prepared by electrophoretic deposition, Advanced Materials 21 (2009) 1756–1760.
[25] K.A. Dean, T.P. Burgin, B.R. Chalamala, Evaporation of carbon nanotubes during electron field emission, Applied Physics Letters 79 (2001) 1873–1875.
[26] A. Pandey, A. Prasad, J.P. Moscatello, Y.K. Yap, Stable electron field emission from PMMA-CNT matrices, ACS Nano 4 (2010) 6760–6766.
[27] S.T. Purcell, P. Vincent, C. Journet, V.T. Binh, Hot nanotubes: stable heating of individual multiwall carbon nanotubes to 2000 K induced by the field-emission current, Physical Review Letters 88 (2002) 105502.
[28] R.H. Fowler, L. Nordheim, Electron emission in intense electric fields, Proceedings of the Royal Society of London Series A 119 (1928) 173–181.
[29] X.H. Ji, Q.Y. Zhang, S.P. Lau, H.X. Jiang, J.Y. Lin, Temperature-dependent photoluminescence and electron field emission properties of AlN nanotip arrays, Applied Physics Letters 94 (2009) 173106.
[30] S.D. Gardner, C.S.K. Singamsetty, G.L. Booth, G.R. He, C.U. Pittman Jr., Surface characterization of carbon fibers using angle-resolved XPS and ISS, Carbon 33 (1995) 587–595.
[31] S. Delpeux, F. Beguin, R. Benoit, R. Erre, N. Manolova, I. Rashkov, Fullerene core star-like polymers—1. Preparation from fullerenes and monoazidopolyethers, European Polymer Journal 34 (1998) 905–915.
[32] R. Bertoncello, A. Casagrande, M. Casarin, A. Glisenti, E. Lanzoni, L. Mirenghi, E. Tondello, Tin, Tic and Ti(C, N) film characterization and its relationship to tribological behaviour, Surface and Interface Analysis 18 (1992) 525–531.
[33] P. Sundberg, R. Larsson, B.J. Folkesson, On the core electron binding energy of carbon and the effective charge of the carbon atom, Journal of Electron Spectroscopy and Related Phenomena 46 (1988) 19–29.
[34] D. Rats, L. Vandenbulcke, R. Herbin, R. Benoit, R. Erre, V. Serin, J. Sevely, Characterization of diamond films deposited on titanium and its alloys, Thin Solid Films 270 (1995) 177–183.
[35] A.C. Ferrari, J.C. Meyer, V. Scardaci, C. Casiraghi, M. Lazzeri, F. Mauri, S. Piscanec, D. Jiang, K.S. Novoselov, S. Roth, A.K. Geim, Raman spectrum of graphene and graphene layers, Physical Review Letters 97 (2006) 187401.
[36] G. Kim, B.W. Jeong, J. Ihm, Deep levels in the band gap of the carbon nanotube with vacancy-related defects, Applied Physics Letters 88 (2006) 193107.
[37] G. Wei, Emission property of carbon nanotube with defects, Applied Physics Letters 89 (2006) 143111.